ELSEVIER

NeuroImage

www.elsevier.com/locate/ynimg
NeuroImage 34 (2007) 1577–1587

Technical Note

A new toolbox for combining magnetoencephalographic source analysis and cytoarchitectonic probabilistic data for anatomical classification of dynamic brain activity

Jürgen Dammers,[a,*] Hartmut Mohlberg,[a] Frank Boers,[a] Peter Tass,[a,b,c,d] Katrin Amunts,[a,c,e] and Klaus Mathiak[e]

[a]*Institute of Medicin, Research Center Jülich GmbH, 52425 Jülich, Germany*
[b]*Virtual Institute of Neuromodulation, Research Center Jülich, 52425 Jülich, Germany*
[c]*Brain Imaging Center West (BICW), Jülich, Germany*
[d]*Department of Stereotaxic and Functional Neurosurgery, University Hospital, 50924 Cologne, Germany*
[e]*Department of Psychiatry and Psychotherapy, RWTH Aachen University, Germany*

Received 9 June 2006; revised 5 September 2006; accepted 26 September 2006
Available online 21 December 2006

Size and location of activated cortical areas are often identified in relation to their surrounding macro-anatomical landmarks such as gyri and sulci. The sulcal pattern, however, is highly variable. In addition, many cortical areas are not linked to well defined landmarks, which in turn do not have a fixed relationship to functional and cytoarchitectonic boundaries. Therefore, it is difficult to unambiguously attribute localized neuronal activity to the corresponding cortical areas in the living human brain. Here we present new methods that are implemented in a toolbox for the objective anatomical identification of neuromagnetic activity with respect to cortical areas. The toolbox enables the platform independent integration of many types of source analysis obtained from magnetoencephalography (MEG) together with probabilistic cytoarchitectonic maps obtained in postmortem brains. The probability maps provide information about the relative frequency of a given cortical area being located at a given position in the brain. In the new software, the neuromagnetic data are analyzed with respect to cytoarchitectonic maps that have been transformed to the individual subject brain space. A number of measures define the degree of overlap between and distance from the activated areas and the corresponding cytoarchitectonic maps. The implemented algorithms enable the investigator to quantify how much of the reconstructed current density can be attributed to distinct cortical areas. Dynamic correspondence patterns between the millisecond-resolved MEG data and the static cytoarchitectonic maps are obtained. We show examples for auditory and visual activation patterns. However, size and location of the postmortem brain areas as well as the inverse method applied to the neuromagnetic data bias the anatomical classification. Therefore, the adaptation to the respective application and a combination of the objective quantities are discussed.

Keywords: Magnetoencephalography; MEG; Cytoarchitecture; Atlas; Human brain mapping; Auditory cortex; Visual cortex

* Corresponding author. Fax: +49 2461 61 2820.
E-mail address: J.Dammers@fz-juelich.de (J. Dammers).
Available online on ScienceDirect (www.sciencedirect.com).

1053-8119/$ - see front matter © 2006 Elsevier Inc. All rights reserved.
doi:10.1016/j.neuroimage.2006.09.040

Introduction

Magnetoencephalographic recordings provide information about the dynamics of neural responses within milliseconds time resolution, but the capabilities in localizing the underlying neuromagnetic activity are limited. In many MEG and other functional imaging studies, an activated cortical area is specified by its relation to the surrounding gyral and sulcal landmarks. For the anatomical interpretation of the functional active areas, the classical Brodmann map (Brodmann, 1909) (as part of the atlas of Talairach and Tournoux; see Talairach and Tournoux, 1988) is still widely used, although this map does not take the considerable intersubject variability into account. Previous studies have reported that it is difficult to identify functional data in relation to their anatomical landmarks, even after spatial normalization (Zeki et al., 1991; Tootell et al., 1995; Dumoulin et al., 2000). Moreover, many cortical areas are not provided with well defined landmarks, but show high variability in the sulcal and gyral pattern across subjects (MCCarthy et al., 1995; Anderson et al., 1996; Amunts et al., 2000). It remains therefore difficult to unequivocally attribute the location or foci of the activation with respect to cortical areas.

Cytoarchitectonic analysis of postmortem human brains provides the exact borders of a given cortical area on a microscopic level (Schleicher et al., 1999; Amunts and Zilles, 2001; Zilles et al., 2002) and is closely associated with functional specialization (Brodmann, 1914; Roland and Zilles, 1998; Luppino et al., 1991; Matelli et al., 1991; Passingham et al., 2002). Previous studies of our group showed that neuroanatomical landmarks do not have a fixed relationship to cytoarchitectonic boundaries; and their gyri and sulci may vary independently from borders of cortical areas (Zilles et al., 1997; Amunts et al., 1999, 2000; Grefkes et al., 2001; Morosan et al., 2001; Rademacher et al., 2001).

Cytoarchitectonically defined anatomical stereotaxic maps are based on a probabilistic approach and have been introduced about

ten years ago (Roland and Zilles, 1994, 1998; Amunts and Zilles, 2001; Zilles et al., 2002). They include, for instance, maps of cortical areas of the motor, somatosensory, auditory, visual cortex and language-related regions (www.fz-juelich.de/ime/ime_probability_maps). The three-dimensional probability maps provide information about the relative frequency of a cortical area located at a given position in the stereotaxic space of the reference brain. In the last few years, such maps have been successfully applied in functional imaging studies using PET (Geyer et al., 1996, 2001; Indefrey et al., 2001; Larsson et al., 2002; Horwitz et al., 2003; Young et al., 2003), fMRI (Binkofski et al., 2000; Grefkes et al., 2002; Amunts et al., 2004; Wilms et al., 2005; Eickhoff et al., 2006) and MEG (Barnikol et al., 2006) improving significantly the analysis of the structural and functional relationship in the human brain.

Recently, a new statistical parametric mapping (SPM; http://www.fil.ion.ucl.ac.uk/spm) toolbox was presented by our group, which uses cytoarchitectonic maps to correlate activation foci obtained from functional imaging data (Eickhoff et al., 2005; http://www.fz-juelich.de/ime/spm_anatomy_toolbox) in a common reference space. For magnetoencephalographic data with its specific properties, such a tool is not yet available. With the introduction of SPM5, it is now possible to analyze data from electroencephalographic (EEG) and magnetoencephalographic (MEG) recordings within the same framework. However, the SPM Anatomy toolbox (the current version is linked to SPM2) introduced by Eickhoff et al. (2005) was designed to assign static functional foci derived from fMRI data to a common reference brain. In contrast, our software package *MEG Anatomy toolbox* is capable of linking the vector valued neuromagnetic activation to cytoarchitectonic probabilistic maps onto the reference brain from the Montreal Neurological Institute (MNI) and the individual subject brain. Moreover, the toolbox will be enhanced to serve for EEG data as well. Further extensions – such as realistic head modeling and support of other data formats – are currently pursued. In our recent study (Barnikol et al., 2006), using a preliminary version of our software, we demonstrated results from magnetoencephalographic recordings mapped together with cytoarchitectonic probability maps onto the individual subject brain space. These maps served as an individual anatomical reference for neuromagnetic activations.

With the *MEG Anatomy toolbox*, we specifically emphasize the excellent time resolution of MEG, such that all measures can be analyzed as a function of time. Furthermore, the routines measure the statistical properties of the neuromagnetic data and the corresponding cytoarchitectonic maps and provide an assignment of the active areas to anatomical structure. This paper describes in detail the main features of the *MEG Anatomy toolbox*:

i. Display of neuromagnetic data (current density distributions as well as dipoles) on top of individual MRI scans and individual probabilistic maps.
ii. Statistical analysis of the neuromagnetic data with respect to the probabilistic cytoarchitectonic maps (individual subject brain space as well as MNI reference space, http://www.bic.mni.mcgill.ca), and to cytoarchitectonic maps of individual post-mortem brain areas that form the basis of the probabilistic maps (reference space).
iii. Various measures that quantify the degree of overlap of activation patterns and the probabilistic cytoarchitectonic maps.
iv. Various distance measures between activation and areas defined by cytoarchitectonic maps.
v. High time resolution analysis of neuro-functional overlap and distance measures.

Methods and results

We have used the programming language IDL (Interactive Data Language) from Research Systems Inc. (RSI, Boulder, CO 80301, USA, http://www.rsinc.com) for developing our platform-independent software *MEG Anatomy toolbox*. The toolbox was written using IDL version 6.2 without any additional extensions required. The current version of the *MEG Anatomy toolbox* can handle two types of reconstructed MEG data to correlate with probabilistic cytoarchitectonic maps: (i) volumes of reconstructed current densities with scalar or vector valued information; and (ii) results from single or multiple current dipole fits.

In order to demonstrate the functionality of the MEG Anatomy toolbox, we use examples from distributed source analysis as well as examples obtained from a dipole analysis providing point like sources.

MEG data set examples

To demonstrate the functionality of the *MEG Anatomy toolbox*, we use results from an auditory tone burst and visual pattern reversal experiment. Three healthy male volunteers (age: 31, 42 and 44 years) participated in the MEG experiments. All subjects had either normal or corrected-to-normal visual acuity. Participation in this MEG experiment was in accordance with the Institutional Committee on Human Research. All volunteers gave their informed consent after explanation of the procedure and the purpose of the experiment.

For the auditory experiment, 300 binaural stimuli (1 kHz, 50 ms duration, randomized ISI with a mean of 1.5 ± 0.5 s) were presented. The same number of stimuli were applied with the same ISI in the visual pattern reversal experiment (single check size of 3.8°, Michelson contrast = 0.98). Auditory and visually evoked fields were recorded using the 4D-Neuroimaging Magnes 2500 system, a whole head magnetometer with 148 channels.

The neuromagnetic activity was continuously recorded with a sampling rate of 1017.25 Hz and a bandwidth from 0.1 to 400 Hz. Magnetic fields induced by the subject's heart beat and eye blinks were removed by means of independent component analysis (Bell and Sejnowksi, 1995; Jahn et al., 1998; Vigario et al., 2000). The time of the stimulus onset was corrected by the delay of the presentation devices (30 ms and 18 ms delay for the auditory and visual presentation, respectively). After semi-automated artifact rejection, the signals were averaged to the onset of the stimuli using a time window of 300 ms before and 500 ms after stimulus onset. Finally, the averaged responses were band-pass filtered in the frequency domain from 1 to 40 Hz.

Coregistration of MRI and MEG

The subject's scalp was digitized with some thousands of points using a 3D digitizer (Polhemus, 3Space/Fastrak, USA). For further mapping with the individual MRI, high resolution T1-weighted MR images were acquired for each subject using a 1.5-T Siemens Sonata Vision system. The pixel size for each of the T1-weighted sagittal section was 1×1 mm^2 with a slice spacing of 1.0 mm. The computed head shape was matched to the surface of the scalp by means of custom software, providing a transformation matrix between the MEG head coordinate and MRI coordinate system.

Source analysis

For reconstruction of distributed sources, we used magnetic field tomography (MFT), which estimates the primary current density $\mathbf{j}(\mathbf{r},t)$, where $\mathbf{r}$ denotes the spatial coordinates (a voxel at location $\mathbf{r}$) within the source space at time t (Ioannides et al., 1990, 1994; Taylor et al., 1999). MFT provides vector valued volumes of reconstructed current densities using a grid spacing of about 10 mm or below (depending on the size of the brain).

A baseline correction was performed based on the prestimulus interval t_{pre} ranging from −300 ms to 0 ms. The 99th percentiles of the distribution of $||\mathbf{j}(\mathbf{r},t_{pre})||$ served as confidence level for $||\mathbf{j}(\mathbf{r},t)||$ to detect only responses which exceed the prestimulus baseline level. Three hemispherical source spaces were used for each subject covering the either the left or the right hemisphere or the occipital part of the brain. MFT was then applied separately using 90 channels located closest to each of the source space. In order to extract brain areas displaying significant activity in every subject, regions of interest (ROI) were identified based on the baseline corrected modulus of the current densities $||\mathbf{j}(\mathbf{r},t)||_{bc}$. in the post-stimulus time interval and at the locations around the local spatial maximum. Since the spatial expansion of the reconstructed current source densities may considerably differ in size (depending, e.g., on the signal-to-noise ratio and the source depth), we used a cut-off threshold of 80% of the ROI's maximal activity. Thereby, we obtained ROIs of peak activations for further correlation with corresponding anatomical structure.

In addition, a single current dipole analysis (built-in software from 4D-Neuroimaging, San Diego, USA, http://www.4dneuroimaging.com) was applied to a few examples of data for demonstrating some of the features implemented in the *MEG Anatomy toolbox* that are designed for point-like sources.

Probabilistic cytoarchitectonic maps

In order to anatomically identify active generators underlying auditory or visual evoked magnetic fields, we applied the cytoarchitectonic probabilistic maps of the following visual and auditory cortical areas: BA 17, BA 18 (Amunts et al., 2000), hOc4v and hOc3v (Rottschy et al., 2005), hOc5 (Malikovic et al., in press) and Te1 (Morosan et al., 2001) as the cytoarchitectonic correlates of human V1, V2, V4(v) (v indicates the ventral part), VP, V5/MT+ and the primary auditory cortex (AI), respectively. For the analysis of the auditory evoked activity, we considered three subdivisions from Te1: Te1.1, Te1.0 and Te1.2, which are located along the mediolateral axis of the Heschl's gyrus (Morosan et al., 2001).

The cytoarchitectonic analysis was obtained from the body donor program of the Institute of Brain Research, Heinrich Heine University of Düsseldorf, Germany (for details, see Amunts et al., 2000; Zilles et al., 2002). In short, cytoarchitectonic mapping was performed in 10 adult human postmortem brains. Images of histological sections were acquired. They were 3D reconstructed using high resolution MR images of the brains before embedding in paraffin and histological processing. Affine as well as non-linear elastic transformation was applied to warp the histological volumes to the T1-weighted single subject template of the Montreal Neurological Institute (MNI; Evans et al., 1993; Collins et al., 1994; Holmes et al., 1998). The warping algorithm was accomplished by a fast and automated multigrid elastic transformation (Henn et al., 1997; Mohlberg et al., 2002, 2003; Hömke, 2006).

Cytoarchitectonic parcellation was performed using an observer-independent approach (Schleicher and Zilles, 1990; Schleicher et al., 1999) based on objective measures of the cortical profile. The method has been described in detail in several publications reporting the results of cytoarchitectonic mapping (e.g., Amunts et al., 1999, 2000, 2004; Grefkes et al., 2001; Morosan et al., 2001).

The delineated areal borders of the individual postmortem brains were then 3D reconstructed and warped into the format of the MNI standard reference brain. The superposition of the individual cortical areas in the common reference space enables the calculation of the probabilistic cytoarchitectonic maps. These statistical maps can be color coded, where each voxel in this map provides the relative frequency of individual postmortem brains that share the same voxel.

Combining MEG and cytoarchitectonic maps

For display purpose, all data volumes were resliced to a common voxel size of $1\times1\times1$ mm^3. The volumes containing the delineated areas were then warped to the format of the individual MRI of each subject. The applied transformation procedure has been shown to provide accurate registration at a resolution of $1\times1\times1$ mm^3 (Amunts et al., 2004; Hömke, 2006). Mapping the probabilistic cytoarchitectonic maps from the standard reference space onto the individual MRI was computational less demanding than the transfer of the vast amount of spatiotemporal sequences of MFT reconstructions to the common reference space. Moreover, it enabled structural–functional analysis with respect to the macro-anatomy of the individual in vivo brain.

Application and results from MEG anatomy toolbox

Statistical description of visual postmortem maps and probabilistic cytoarchitectonic maps in MNI space

The probabilistic maps are based on cytoarchitectonic analysis of 10 postmortem brains. Each voxel in the probabilistic maps represents the frequency of how many postmortem brains share the same voxel. In order to investigate the intersubject variability of the postmortem data, the volume and the center of gravity was computed for each cortical area. To reflect the variability in the location of the areas, the distance from each center of gravity to the mean center of gravity (across ten postmortem maps) was calculated.

A large volume in the 10% probability map reflects high intersubject variability in size and/or location of the cortical areas. Due to this intersubject variability, the volume of the 10% probability map may exceed the mean volume across the areas of the postmortem brains by a few times (Fig. 1). In contrast, the 100% probability map (the part of the probability map, where all 10 postmortem brains share the same voxels) may contain a few voxels only or even none (cf. red voxels in transversal slices of Fig. 1). The volumes of the 100% probability maps differ between cortical areas. For example, a larger number of postmortem brains share the same voxels in V1 as compared to area V2. The highest probability level obtained in V5 is 60% and 70% for the left and the right hemisphere, respectively, with less than 10 voxels each. It is therefore ambiguous to select a threshold for the probabilistic map for superposition with functional data without considering the distribution of the postmortem data. Table 1 lists the mean volume sizes of different areas from the 10 postmortem brains and the volume size of the corresponding probability map which was closest to this mean volume.

The mean volume of the cytoarchitectonically defined V5 is more than 25 times smaller than that of V1 and V2. The corres-

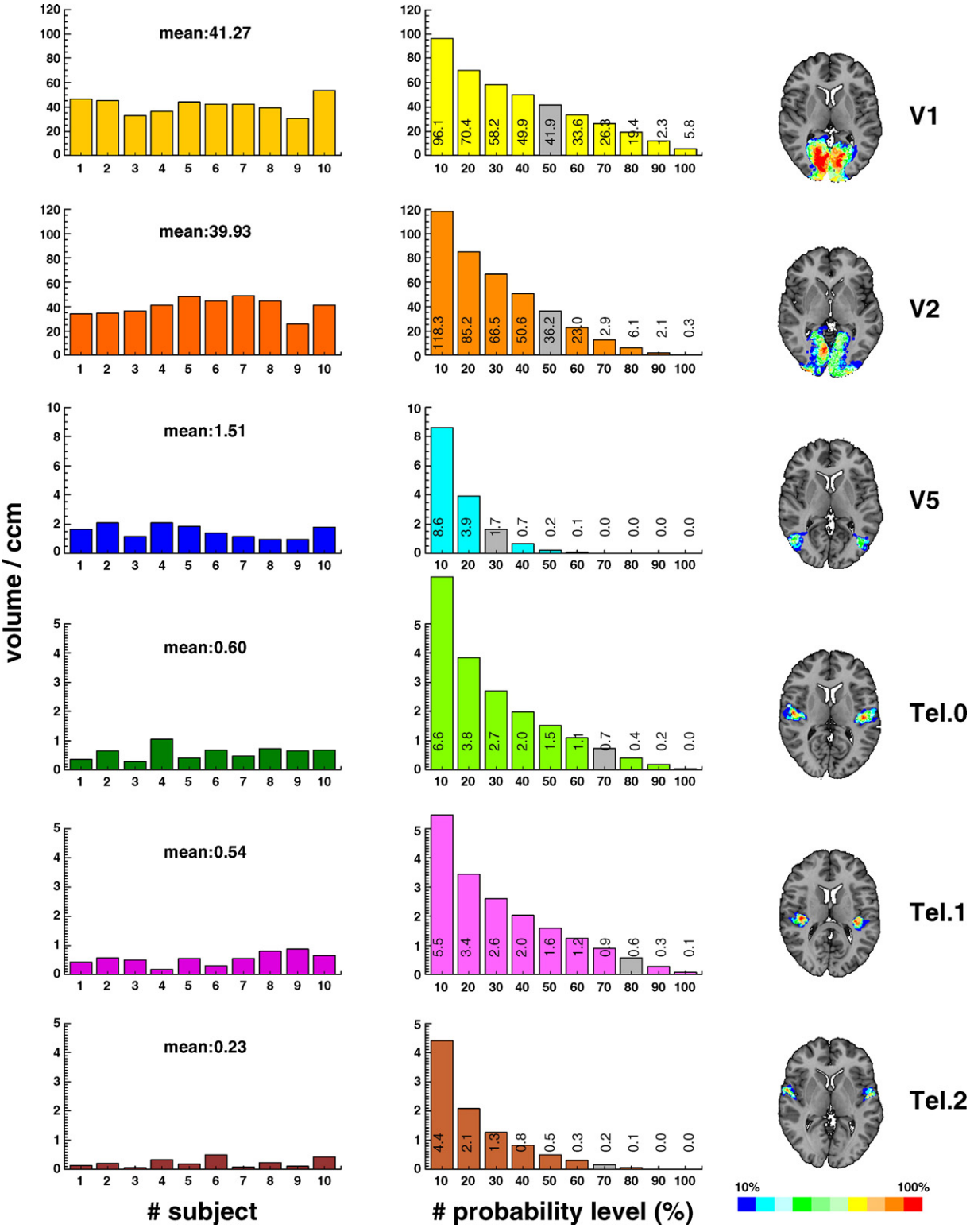

Fig. 1. Volume sizes for different visual areas in MNI space. Left column shows the volume for each area measured in ten postmortem brains. The next column displays the volume of the probabilistic maps for different probability levels. All volume sizes are calculated across both hemispheres. For V5 and Te1, the average volume across both hemispheres is displayed. The gray bars indicate the probability level that agrees best with the mean volume of the postmortem maps (see left column). The right column shows axial slices of the probability map V1, V2, V5, Te1.0, Te1.1 and Te1.2, superimposed on the MNI reference brain. The color bar at the bottom of the right column indicates the number of overlapping postmortem brains for each voxel.

Table 1
Group mean volumes of areas calculated from 10 postmortem brains and the volume of the corresponding probability map

Volume [cm^3]				
	Postmortem		Probability map	
	Area	Mean volume	SD	Volume	Level
Visual				
	V1	41.27	6.83	41.90	50
	V2	39.93	7.25	36.16	50
	V5	1.51	0.44	1.66	30
Auditory				
	Te1.0	0.77	0.21	0.97	30
	Te1.1	0.59	0.24	0.77	30
	Te1.2	0.39	0.16	0.25	30

SD denotes the standard deviation. All volume sizes are averaged across both hemispheres, except for area V1 and V2, where the left and the right sides are taken together.

ponding probability map of V5 shows a larger variability in volume the one of V1 and V2. The relative standard deviation (SD) for area V5 is largest (about 30%) as compared to the other visual areas (relative SD is about 20% or less). The intersubject variability of the postmortem volumes of the primary auditory cortex is more than 30% as expressed by the standard deviation of Te1.0, Te1.1 and Te1.2. Considering existing differences in intersubject variability, we suggest to select the threshold for the probability map, at which the volume size of the map is closest to the mean volume of the area from the ten postmortem brains.

The probability level which agrees best with the sizes of the mean volumes are listed in Table 1 (cf. Fig. 1).

The spatial overlap between an area of a single postmortem brain and its corresponding probabilistic map is 100% only at a probability level of 10%. This is because all voxels of the 10 areas from the postmortem brains were used for the construction of the probability maps. If the neuromagnetic activation would be perfectly reconstructed in a way that for each activated area one would extract a confined ROI which fully lies within the cortical area. How much overlap between the ROI and the probabilistic map can then be expected? Clearly, this depends on the probability level used. In our recent study (Barnikol et al., 2006), we showed group mean overlaps between 10 postmortem visual areas (V1, V2 and V5 only) and the corresponding probability maps were determined for different probability thresholds.

In order to assess the amount of overlap for each of the probability map level, we construct a reference overlap with the areas of the 10 postmortem brains (in MNI space) serving as a replacement for an activated area. A voxel-based overlap calculation is applied for all areas and all probability map thresholds. For each area we calculated a group average overlap in relation to the probability map threshold; the reference volume was fixed to the size of the probability map. The group means overlap value of area V5, for example, is about 8% only at a probability map threshold of 50%. In contrast, area V1 shows a remarkable mean overlap of about 55% at a probability level of 70%. This larger variability of area V5 is also reflected by the relatively high standard deviation (about 30%) of the volume size (cf. Table 1). When choosing a probability map threshold at which the volume size of the probability map resembles best the mean volume size of the areas from the postmortem brains, then the group mean overlap is at least 30% or more. Group mean overlap values are listed in Table 2 for the selected visual and auditory areas.

Maximum probability map

When mapping probabilistic maps of different areas, one problem is that there may be considerable overlap between two neighboring areas. Especially for low probability thresholds, the amount of overlap between two or more probabilistic maps is high. This makes it difficult or even impossible to unequivocally assign functional data to anatomical structure. Increasing the probability map threshold to the mean volume size of the area from the postmortem brains reduces the overlapping effect but may not eliminate it. To overcome this problem, Eickhoff and colleagues (2005) introduced the maximum probability map (MPM), which defines the most likely cytoarchitectonic area at each voxel. All available probabilistic maps from different cytoarchitectonic areas are combined providing one non-overlapping probability map. Voxels are assigned to that area of the MPM, which show the maximum probability. In cases where equal probability is found the voxel in question is assigned to that area which shows the highest average probability in a $3 \times 3 \times 3$ neighborhoods. In rare cases, if the procedure fails to assign a voxel to a certain area, the cube size can be either increased, or as suggested by Eickhoff et al. (2005), the procedure is repeated on smoothed probability maps using an isotropic Gaussian kernel. In addition, the MPM can be considered to provide an appropriate anatomical region for testing the anatomical hypotheses in functional neuroimaging (Eickhoff et al., 2006). It should however be noted that probabilistic maps are not available for the entire cortex and the described approach may overestimate the spatial extent of a delineated area at its borders towards unmapped cortex.

The algorithm for generating MPMs is also implemented in the *MEG Anatomy toolbox*, with the only modification that we use the mean volume size of the areas from the postmortem brains to serve as a threshold for the probability maps. The advantage of using the maximum probability map is that for each individual subject one can construct a multi-area non-overlapping probabilistic map. Such a map may be of interest when activity is detected at the border of two or more cortical areas. In Fig. 2, we show neuromagnetic activity mapped onto the maximum probability map including the visual probability maps of V1, V2, V4(v), VP and V5. In this example (cf. Fig. 2a), the current density ROI is distributed around the border of V1 and V2; however, the activity can assigned clearly, by means of the MPM (cf. Table 3).

Anatomical identification of neuromagnetic data

MEG data (i.e., cerebral current density or current dipoles) are mapped to probabilistic maps in order to correlate structure with function. This is done descriptively by means of visual inspection. In addition to display functional and structural data, the *MEG Anatomy toolbox* is to provides a tool for the quantitative or qualitative analysis of anatomical localization of neuromagnetic data by derived measures. Different overlap and distance measures provide information on how much of the activity can be attributed to cortical areas

Table 2
Group mean overlap values for auditory and visual areas at a probability map threshold, where the volume of the map resembles the mean volume sizes of the areas from the postmortem brains

	V1	V2	V5	Te1.0	Te1.1	Te1.2
Level %	50	50	30	30	30	30
Overlap %	76	57	40	49	51	22

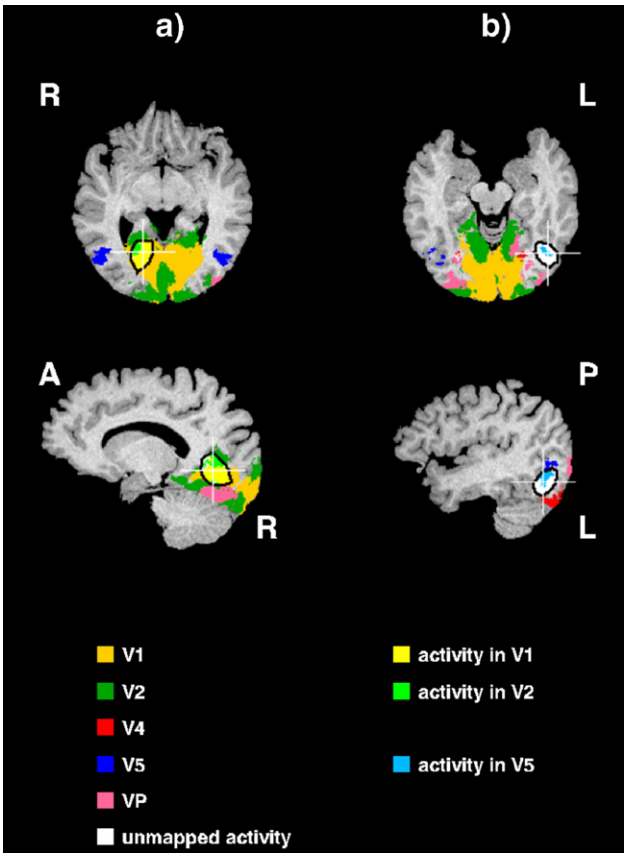

Fig. 2. Superposition of neuromagnetic activity from two subjects on the maximum probability map including the probabilistic maps of V1, V2 and V5. The thresholds for the maps were chosen to fit the group mean area size of the 10 postmortem brains. The white cross hair indicates the location of the ROI's maximal activity. (a) The activation of a single subject at time $t=100$ ms is displayed on top of the visual probabilistic maps of V1 and V2. The black outline indicates the border of the ROI. The overlap of the activity with area V1 (yellow) and V2 (light green) is 55% and 33%, respectively. Unmapped activity is plotted in red. The overlap value for the other visual areas (V4(v), VP and V5) is 0% or less than 1%. (b) The overlap of the neuromagnetic activity at $t=132$ ms with area V5 on the left hemisphere (light blue) from the same subject is 52% (cf. Table 3).

in question. In the following, we will systematically introduce some relevant measures for the functional–anatomical relationship.

ROI labeling for distributed current density

Voxel-based overlap. To quantify the degree of overlap between a region of interest and the MPM, we count all voxels from the ROI that are enclosed within the probability map of each area. The relative overlap is then calculated by dividing the number of common voxels by the number of voxel of the reference volume. To ensure a "fair" comparison, the reference volume is the smaller volume. For example, the majority of the activation shown in Fig. 2a is located in V1 with an overlap fraction of 55% and 33% for area V1 and V2, respectively, while for 12% of the ROI volume the activity is assigned to a region that has not yet been mapped cytoarchitectonically. The example displayed in Fig. 2b shows that the neuromagnetic activation can be assigned to area V5 on the left hemisphere. The overlap between the V5 activation and its probabilistic map is 52%, which is even 12% more than the group mean overlap of the postmortem brains. From the example shown in Fig. 2, some of the statistical measures provided by the *MEG Anatomy toolbox* are listed in Table 3.

Due to the cut-off threshold of 80% maximal activity, the ROIs focus is on strong (evoked-like) activities only. It should be noted that for estimating the overlap some cut-off threshold for the distributed type of neuromagnetic activity, as revealed by MFT (Ioannides et al., 1990), sLoreta (Pascual-Marqui, 2002) or MNE (Hämäläinen et al., 1993; Hämäläinen and Ilmoniemi, 1994), is necessary since the current density is non-zero within the defined source space (e.g., the brain). This cut-off threshold however has a direct influence on the overlap calculation. Therefore, without any additional measures the overlap calculation may be over- or underestimated. However, the voxel-based overlap calculation determines the proportional volume overlap and is therefore applicable for both weak and strong activated clusters.

Mean probability. For each area that overlaps with the selected ROI, the mean probability of the underlying probabilistic map is calculated. For the activity displayed in Fig. 2a, the mean probability p_m is 77% and 42% for area V1 and V2, respectively (cf. Table 3). Since the mean value does not account for the size of the overlapping region, this quantity may be over- or underestimated in cases, where the relative overlap is small (cf. Fig. 2a activity in VP). To compensate for small numbers of overlapping voxels, a normalized mean value p_n is calculated: the sum of the probability values for each overlapping area is divided by the total number of voxel of the reference volume (e.g., the ROI). In the example shown in Fig. 2a, the normalized mean probability p_n for the activity within V1 is 42%, whereas for the V2 and VP activation the p_n value drops down to 14% and <1%, respectively, due to the small number of overlapping ROI voxels (Table 3).

Activity-weighted overlap. In cases where the source reconstruction reveals two or more activation clusters, it may be of interest to compare the amount of activity between all activated clusters in order to distinguish weak from strong activations. Therefore, the overlap calculation can be weighted by the strength of the current density at each voxel. The same routine may also be

Table 3
Statistical measures provided by the *MEG Anatomy toolbox*

	V1	V2	V4(v)	VP	V5
ROI (a)					
Overlap [%]	55	33	0	<1	0
ROI activity [%]	55	33	0	<1	0
p_m [%]	77	43	0	35	0
p_n [%]	42	14	0	<1	0
Prmax [%]	0	80	0	0	0
Prcom [%]	70	0	0	0	0
ROI (b)					
Overlap [%]	0	0	0	0	52
ROI activity [%]	0	0	0	0	27
p_m [%]	0	0	0	0	37
p_n [%]	0	0	0	0	9
p_{rmax} [%]	0	0	0	0	30
p_{rcom} [%]	0	0	0	0	40

The results of this table refer to the example shown in Fig. 2. ROI (a) and ROI (b) indicate the ROI shown in Figs. 2a and b, respectively. p_m and p_n are the mean probability and the normalized mean probability within the overlapping region, respectively. p_{rmax} and p_{rcom} are the probability at the ROIs maximal location and the location of the ROI center of mass, respectively.

utilized if the activation is located in more than one cortical area. The weighted overlap calculation provides information about the relative amount of current found in each area. The cortical areas are labeled based on the strength of the activations.

Probability-weighted ratios of activity. Alternatively to the labeling based on the strength of the current density, the neuromagnetic activation can be weighted by the probability of the underlying probabilistic maps. Activation clusters are sometimes fairly widespread and may be distributed across more than one cortical area. If the spatial variation of the strength of the current density within the cluster is sufficiently small, it would be difficult to label the activation based on an amplitude like threshold, since the amount of activity would depend on the number of overlapping voxels for each area only. For such cases, it is possible to integrate the activity within each area without using any threshold for the strength of the current density. After integration, the activity is weighted with the probability of the entire probabilistic maps (i.e., no threshold is applied for the probability level). For unmapped activity (i.e., regions where probabilistic maps are not yet available), the weights are set to zero and the sum of all weights is 1. Ratios of the probability-weighted activity can be constructed to investigate, which area is the most likely activated area (cf. Barnikol et al., 2006).

ROI labeling for point-like sources. Neuromagnetic data can be reconstructed in different ways depending on the inverse method applied. Hence, the output format of the reconstructed activity can differ significantly. For example various reconstruction methods provide three-dimensional current density vectors for each point in space (and time). The data may be visualized using vector valued data (e.g., MFT, Ioannides et al., 1990) or scalar values representing the strength of the current density (sLoreta, Pascual-Marqui, 2002). Other inverse methods reconstruct the underlying activity by using a single current dipole (4-D Neuroimaging, 1999) or multiple current dipole modeling (Mosher and Leahy, 1992, 1998; Scherg and Berg, 1996). A typically output of a dipole analysis is the location and orientation of the current dipole(s) that best explains the measured neuromagnetic data. The location of such point-like sources represents an activated cortical region with some statistical measures like the goodness of fit (GoF) value describing the (un)certainty of the current dipole fit.

The GoF value g ranges from 0 to 1 and describes how well the measured field agrees with the estimated field of the dipole analysis, in terms of a least square estimate. The model fully agrees in the case of $g=1$ (for detailed description, we refer to Hämäläinen et al., 1993). Fig. 3 illustrates an example of a dipole analysis using the software from 4D Neuroimaging (4-D Neuroimaging, 1999). The dipole with the largest g value (at time 70 ms) within the time range of 50–120 ms was selected. The current dipole is mapped onto the maximum probability map and superimposed onto the individual MRI scan (Fig. 3) of one subject. In the figure, the reconstructed current density (as revealed by MFT) of the same latency is included for comparison with the current dipole estimate. In this example, the dipole analysis revealed a goodness of fit value of 0.99 at latency of 70 ms. The dipole is located within the MFT activation showing ≥80% of the maximal activity. The distance between the dipole location and the location of the maximal MFT activation is 8 mm and 6 mm to the ROIs center of gravity.

In order to examine the probabilistic anatomical location of a dipole (or any other point in space, like the location of the maximal activity or the center of gravity of an activation cluster, from a distributed source analysis), the *MEG Anatomy toolbox* determines the probability of the underlying probability map at the selected location. For the example shown in Fig. 3, the probability values of 80% and 60% are assigned to area Te1.0 at the location of the current dipole and the maximum activity as revealed by MFT, respectively. In cases where the dipole location is close to neighboring areas, the probability value of a single voxel may not be reliable for anatomical identification. Therefore, the mean probability of a volume defined by a sphere with a given radius can be calculated. A diameter of 2 cm for the mean probability calculation around the dipole location results in a mean probability of 79%, 0% and 67% for the areas Te1.0, Te1.1 and Te1.2, respectively. The overlap calculation of the sphere around the dipole reveals 91%, 0% and 28% for the same areas.

Distance measures

Local distance measures. For distributed activation clusters, which may cover several cortical areas, it can be helpful to examine the probabilistic anatomical location of a given point in space. This location may be the ROI's maximal activation, the center of gravity or location points derived from a dipole analysis. For such location points the probability value of the underlying probability map is provided as described above. If the applied source reconstruction reveals location points close to borders of different cytoarchitectonic maps, or the location in question has not yet mapped cytoarchitectonically, the minimal distance *Dmin* to the underlying as well to neighboring cytoarchitectonic maps is determined. This quantity provides estimates about which cortical area is closest to the location in question.

Mean voxel to voxel distance. An additional distance measure, the mean voxel-to-voxel distance *Dmv*, can be calculated for confined regions like the volume of an ROI or a spherical volume around the location of a dipole. For each voxel within this volume the closest distance to the probability map is calculated, revealing n minimal distances to a selected cortical area, where n is the number of voxels within the volume. The mean voxel-to-voxel distance *Dmv* is defined as the average distance across all minimal distances. For *Dmv* values equal to zero the volume (ROI) is fully covered by the probability map. More interestingly, *Dmv* values greater than zero quantify the fractional expansion of the volume that does not overlap with the probability map. For example, an activation cluster may be located at the border of Te1.1 and Te1.2 (cf. Fig. 4). The *Dmv* quantity provides an estimate if and to what extent an activation is unmapped to a given probability map.

Time-dependent evaluation. Since MEG provides excellent time resolution, all measures provided by the *MEG Anatomy toolbox* can be evaluated as time courses. In Fig. 4, we demonstrate how the neuromagnetic activation from an auditory response of the right hemisphere is assigned dynamically to anatomical structure, by means of the mean voxel-to-voxel distance *Dmv*. The selected time range for the analysis was chosen to fit the N100m response of the subject (Fig. 4a). The mean voxel-to-voxel distance *Dmv* was calculated for the areas of the primary auditory cortex Te1.0 (yellow), Te1.1 (green) and Te1.2 (blue) within the selected time range. In Fig. 4b we plot the ROI distance *Dmv* to all three areas. Peaks of each curve indicate the latency of the shortest distance to the corresponding area, in terms of the mean voxel-to-voxel distance. The figure shows that at the beginning of the investigated

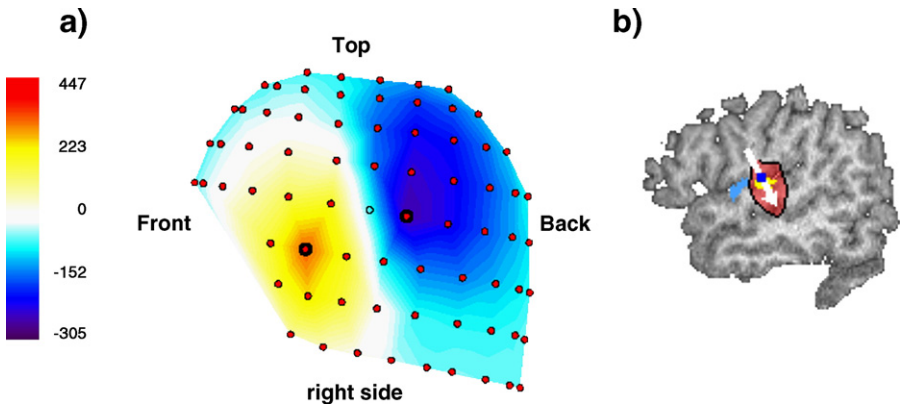

Fig. 3. (a) Contour plot of MEG signals from an auditory response of one subject at a latency of 70 ms after stimulus onset shown for the right hemisphere. The scaling of the color bar is in the femto-Tesla range. (b) Localization of the single dipole fit is superimposed on probabilistic maps of Te1.0 (yellow) and Te1.2 (light blue). The current dipole with the highest goodness of fit (GoF) value was found at 70 ms after stimulus onset from the time range 50 ms–120 ms. The location (blue dot) of the current dipole (white) matches within the region of the probabilistic map of Te1.0 (yellow). For comparison, the reconstruction from MFT analysis is displayed in red at the same latency.

time range, the activation is located closely to area Te1.1 and Te1.0 at latency 58 ms but is then moving towards area Te1.0. The distance of the activation cluster to area Te1.0 is minimal at latency 77 ms; 91 ms after stimulus onset, the activation is localized closest to the region of area Te1.2 and Te1.0 (Fig. 4c).

Discussion

We here present a new software package for the anatomical identification of neuromagnetic data derived from distributed source or dipole analysis. For anatomical labeling, the vector valued or scalar functional data can be mapped onto three-dimensional cytoarchitectonic probabilistic maps (Amunts and Zilles, 2001; Zilles et al., 2002), which have been either transferred to the individual subject brain space or to the MNI standard reference space (Evans et al., 1993; Collins et al., 1994). The new software package enables the analysis of four-dimensional (3D space and time) neuromagnetic data in relation to probabilistic maps of cortical areas with respect to the macro-anatomy of the individual in vivo brain easily, efficiently and on a quantitative basis.

It is computational less demanding to study the relationship of anatomy and function in the individual subject brain space because in contrast to the dynamic MEG data, the probabilistic maps are static. Hence, only one spatial transformation needs to be calculated. In contrast, the functional data derived from MFT (or any other distributed source analysis) comprise typically a few thousand data volumes per measurement. In addition, transforming to the individual subject brain space may be superior, if the anatomy of the particular brain has to be kept unchanged (e.g., in patients). However, for group analysis of functional data, the software is capable of transforming selected data volumes of the current densities or coordinates from a dipole analysis into the standardized MNI reference space.

In contrast to the SPM Anatomy toolbox for fMRI, which has been introduced recently by our group (Eickhoff et al., 2005), the new toolbox exploits the advantage of MEG, which provides excellent time resolution. All quantities provided by the software, like overlap statistics and distance measures to anatomical probabilistic maps, can be investigated over time (Fig. 4), thus reflecting the dynamic nature of MEG data.

For the anatomical identification of functionally active foci, we introduced different overlap and distance measures that may be used in dependency on the nature of functional data and the scientific goal. For instance, the spatial extent of overlap may be weighted by the strength of the current density vectors, which is particular of interest if the activity is widespread. Due to the structure of the lead fields, this is prominent for source estimates at deeper brain areas. Moreover, the spatial overlap can be calculated with respect to different reference volumes (ROI of functional data or volume of the probabilistic map, cf. Barnikol et al., 2006). The estimation of the overlap however must be interpreted in relation to the group mean overlap of the 10 postmortem brains with corresponding probability maps (cf. Fig. 1). With increasing probability map thresholds, the group means overlap decreases depending on the cortical areas and thus, reflects different degrees of intersubject variability in the distinct areas.

Previous studies reported a large intersubject variability of the 10 postmortem brains (Amunts et al., 2000; Amunts and Zilles, 2001; Wohlschlager et al., 2005). However, the threshold selection for any single probabilistic map (or the MPM) must not be fix to one value but should be selected under the consideration of the different intersubject variabilities. We here propose to choose a probability map threshold that best fits the group mean volume of the area of interest from the 10 postmortem brains (cf. Table 1).

For all defined ROIs, a mean probability value (within the ROI) of the underlying cytoarchitectonic map expresses the probability of attributing the neuromagnetic activity to this cortical area. To compensate for the over-estimation of this quantity in cases where the spatial extent is a few voxels only; the mean probability value was normalized to the size of the overlapping reference volume. This normalization results in a drop of this quantity and compensates for ROIs with small overlaps with corresponding probabilistic maps (cf. Table 3).

In order to attribute functional data to anatomical structure, in addition to the spatial extent of overlap, the assignments can be based on local and group mean voxel-to-voxel distance measures. Some of the algorithms have already been applied in our previous study (Barnikol et al., 2006). The new toolbox is now capable of investigating such quantities within each functional imaging time interval (cf. Fig. 4). Such a time-dependent evaluation of the

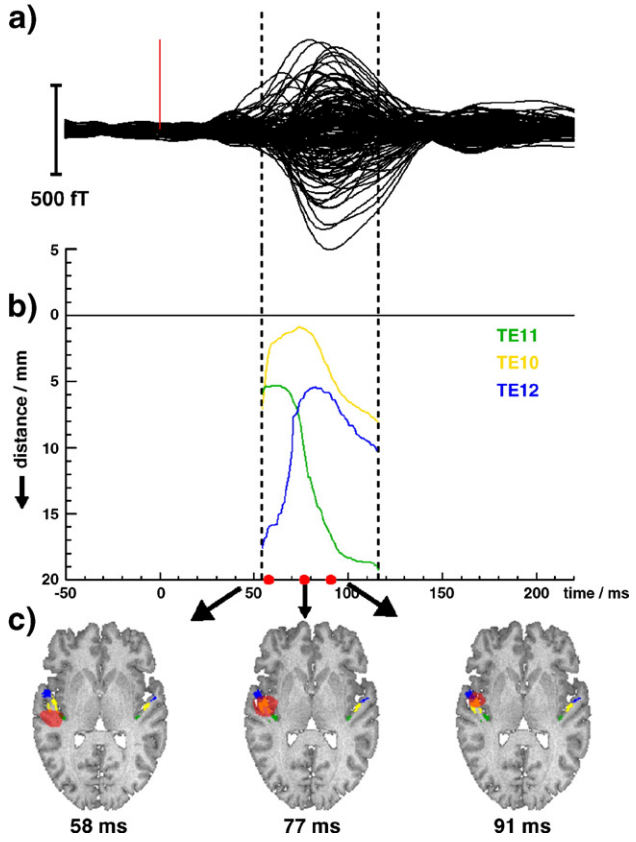

Fig. 4. Distance evaluation of neuromagnetic activity to areas of the primary auditory cortex from the right hemisphere of one subject. (a) The distance calculation was performed for the time range of the auditory N100m response. (b) For the given time range, the mean voxel-to-voxel distance is plotted for the areas of the primary auditory cortex Te1.0 (yellow), Te1.1 (green) and Te1.2 (blue). (c) The reconstructed neuromagnetic activity is plotted in red onto the probabilistic maps of the primary auditory at peak latencies of the distance measure in panel b.

quantities provided by the toolbox may contribute to an understanding of the dynamics of the neuromagnetic data.

It should be noted, that the spatial resolution of the probabilistic maps is much higher (1 mm^3 voxel size, Amunts et al., 2004; Mohlberg et al., 2003) than that of MEG data analysis. The grid size used for MFT reconstruction in the experiments described above was below 10 mm. All quantities provided must therefore be considered within this context to avoid over- or underestimation of probabilities, overlap values and distance measures due to the interpolation procedure. However, the toolbox has no impact on the inverse method applied. Assuming an optimal reconstruction method is available to analyze MEG data, the *MEG Anatomy toolbox* provides measures for the anatomical localization of functional activations.

Eickhoff et al. (2005) introduced the maximum probability map to avoid the problem that two or more architectonic areas may overlap at lower probabilities. In addition, a median probability is calculated at the border zone of two defined areas, serving as a threshold probability for including a voxel into the MPM, which holds non-overlapping volumes of delineated areas. This approach was also implemented in the *MEG Anatomy toolbox*, with the only modification, that the threshold used for the MPM is not fixed but set to the threshold that best fits the group mean volume size of the areas from the 10 postmortem brains. For comparison with results derived from the SPM Anatomy toolbox, it is possible to choose the same probability map thresholds as used by the SPM toolbox. Given that SPM5 enables the MEG/EEG data analysis, our current developments are directed towards an integration of the presented MEG Anatomy toolbox into an updated version of the Anatomy toolbox of SPM.

In summary, we presented a toolbox for the anatomical identification of neuromagnetic activity. With the combination of cytoarchitectonic data and neuromagnetic correlates of distinct visual and auditory areas, the software package enables the simultaneous investigation of anatomical and functional information across time.

The application examples shown above demonstrated the advantage of combining two different methods for source analysis, where magnetoencephalography and cytoarchitectonic data analysis utilize high temporal and high spatial resolution, respectively. Since the combined measures might be biased by variability or size of cortical areas, we suggest combining different approaches to best characterize the dynamic brain patterns. The presented toolbox offers the central elements for a qualitative and quantitative analysis.

Acknowledgments

This Human Brain Project/Neuroinformatics research is funded by the National Institute of Biomedical Imaging and Bioengineering, the National Institute of Neurological Disorders and Stroke and the National Institute of Mental Health. The author K.M. is supported by an AstraZeneca foundation.

References

Amunts, K., Zilles, K., 2001. Advances in cytoarchitectonic mapping of the human cerebral cortex. Neuroimaging Clin. N. Am. 11 (2), 151–169.

Amunts, K., Schleicher, A., Bürgel, U., Mohlberg, H., Uylings, H.B.M., Zilles, K., 1999. Broca's region revisited: cytoarchitecture and intersubject variability. J. Comp. Neurol. 412, 319–341.

Amunts, K., Malikovic, A., et al., 2000. Brodmann's area 17 and 18 brought into stereotaxic space—Where and how variable? NeuroImage 11, 66–84.

Amunts, K., Weiss, P.H., Mohlberg, H., Pieperhoff, P., Eickhoff, S., Gurd, J.M., Marshall, J.C., Shah, N.J., Fink, G.R., Zilles, K., 2004. Analysis of neural mechanisms underlying verbal fluency in cytoarchitectonically defined stereotaxic space. The roles of Brodmann areas 44 and 45. NeuroImage 22 (1), 42–56.

Anderson, S.J., Holliday, I.E., Singh, G.D., Harding, G.F.A., 1996. Localization and functional analysis of human cortical area of V5 using magnetoencephalography. Proc. R. Soc. London, B 263, 423–431.

Barnikol, U.B., Amunts, K., Dammers, J., Mohlberg, H., Fieseler, T., Malikovic, A., Zilles, K., Niedeggen, M., Tass, P.A., 2006. Pattern reversal visual evoked responses of V1/V2 and V5/MT as revealed by MEG combined with probabilistic cytoarchitectonic maps. NeuroImage 31, 86–108.

Bell, A., Sejnowksi, T., 1995. An information-maximization approach to blind separation and blind deconvolution. Neural Comput. 7, 1129–1159.

Binkofski, F., Amunts, K., Stephan, K.M., Posse, S., Schormann, T., Freund, H.-J., Zilles, K., Seitz, R.J., 2000. Broca's region subserves imagery of motion: a combined cytoarchitectonic and fMRI study. Hum. Brain Mapp. 11, 273–285.

Brodmann, K., 1909. Vergleichende Lokalisationslehre der Großhirnrinde in ihren Prinzipien dargestellt auf Grund des Zellenbaues. Barth, JA, Leipzig.

Brodmann, K., 1914. Physiologie des Gehirns. Neue Dtsch. Chir. 11, 85–426.

Collins, D.L., Neelin, P., Peters, T.M., Evans, A.C., 1994. Automatic 3-D intersubject registration of MR volumetric data in standardized Talairach space. J. Comput. Assist. Tomogr. 18, 192–205.

Dumoulin, S.O., Bittar, R.G., Kabani, N.J., Baker, C.L., LeGoualher, G., Pike, G.B., Evans, A.C., 2000. A new anatomical landmark for reliable identification of human area V5/MT: a quantitative analysis of sulcal patterning. Cereb. Cortex 10, 454–463.

Eickhoff, S.B., Stephan, K.E., Mohlberg, H., Grefkes, C., Fink, G.R., Amunts, K., Zilles, K., 2005. A new SPM toolbox for combining probabilistic cytoarchitectonic maps and functional imaging data. NeuroImage 25, 1325–1335.

Eickhoff, S.B., Lotze, M., Wietek, B., Amunts, K., Enck, P., Zilles, K., 2006. Segregation of visceral and somatosensory afferents: an fMRI and cytoarchitectonic mapping study. NeuroImage 31, 1004–1014.

Evans, A.C., Collins, D.L., Mills, S.R., Brown, E.D., Kelly, R.L., Peters, T.M., 1993. 3-D statistical neuroanatomical models from 305 MRI volumes. Nuclear Science Symposium and Medical Imaging Conference, 1993. 1993 IEEE Conference Record, San Francisco, CA, pp. 1813–1817.

Geyer, S., Ledberg, A., Schleicher, A., Kinomura, S., Schormann, T., Burgel, U., Klingberg, T., Larsson, J., Zilles, K., Roland, P.E., 1996. Two different areas within the primary motor cortex of man. Nature 382, 805–807.

Geyer, S., Schleicher, A., Schormann, T., Mohlberg, H., Bodegard, A., Roland, P.E., Zilles, K., 2001. Integration of microstructural and functional aspects of human somatosensory areas 3a, 3b, and 1 on the basis of a computerized brain atlas. Anat. Embryol. 204, 351–366.

Grefkes, C., Geyer, S., Schormann, T., Roland, P., Zilles, K., 2001. Human somatosensory area 2: observer-independent cytoarchitectonic mapping, interindividual variability, and population map. NeuroImage 14, 617–631.

Grefkes, C., Weiss, P.H., Zilles, K., Fink, G.R., 2002. Crossmodal processing of object features in human anterior intraparietal cortex: an fMRI study implies equivalencies between humans and monkeys. Neuron 35, 173–184.

Hämäläinen, M.S., Ilmoniemi, R.J., 1994. Interpreting magnetic fields of the brain: minimum norm estimates. Med. Biol. Eng. Comput. 32, 35–42.

Hämäläinen, M.S., Hari, R., Risto, J., Ilmoniemi, R.J., Knuutila, J., Lounasmaa, O.V., 1993. Magnetoencephalography-theory, instrumentation, and applications to non-invasive studies of the working human brain. Rev. Mod. Phys. 65 (2).

Henn, S., Schormann, T., Engler, K., Zilles, K., Witsch, K., 1997. Elastische Anpassung in der digitalen Bildverarbeitung auf mehreren Auflösungsstufen mit Hilfe von Mehrgitterverfahren. In: Paulus, E., Wahl, F.M. (Eds.), Mustererkennung 1997. Informatik Aktuell, Springer, pp. 392–399.

Holmes, C.J., Hoge, R., Collins, L., Woods, R., Toga, A.W., Evans, A.C., 1998. Enhancement of MR images using registration for signal averaging. J. Comput. Assist. Tomogr. 22 (2), 324–344.

Hömke, L., 2006. A multigrid method for anisotrophic PDE's in elastic image registration. Numerical Linear Algebra with Applications, Anonymous Copper Mountain. John Wiley and Sons, pp. 215–229.

Horwitz, B., Amunts, K., Bhattacharyya, R., Patkin, D., Jeffries, J., Zilles, K., Braun, A.R., 2003. Activation of Broca's area during the production of spoken and signed language: a combined cytoarchitectonic mapping and PET analysis. Neuropsychologia 41, 1868–1876.

Indefrey, P., Brown, C.M., Hellwig, F., Amunts, K., Herzog, H., Seitz, R.J., Hagoort, P., 2001. A neural correlate of syntactic encoding during speech production. Proc. Natl. Acad. Sci. 98, 5933–5936.

Ioannides, A.A., 1994. Estimates of brain activity using magnetic field tomography and large scale communication within the brain. In: Ho, M.W., Popp, F.A., Warnke, U. (Eds.), Bioelectrodynamics and Biocommunication. World Scientific, Singapore, pp. 319–353.

Ioannides, A.A., Bolton, J.P.R., Clarke, C.J.S., 1990. Continuous probabilistic solution to the biomagnetic inverse problem. Inverse Probl. 6, 523–542.

Jahn, O., Cichocki, A., Ioannides, A.A., Amari, S., 1998. Identification and elimination of artifacts from MEG signals using efficient independent component analysis. In: Yoshimoto, T., Kotani, M., Kuriki, S., Karibe, H., Nakasato, N. (Eds.), Proceedings of the 11th International Conference on Biomagnetism, pp. 224–227.

Larsson, J., Amunts, K., Gulyás, B., Malikovic, A., Zilles, K., Roland, P.E., 2002. Perceptual segregation of overlapping shapes activates posterior extrastriate visual cortex in man. Exp. Brain Res. 143, 1–10.

Luppino, G., Matelli, G., Camarda, R.M., Gallese, V., Rizzolatti, G., 1991. Multiple representations of body movements in mesial area 6 and the adjacent cingulate cortex: an intracortical microstimulation study in the macaque monkey. J. Comp. Neurol. 311, 463–482.

Malikovic, A., Amunts, K., Schleicher, A., Mohlberg, H., Eickhoff, S.B., Wilms, M., Palomero-Gallagher, N., Armstrong, E., Zilles, K., in press. Cytoarchitectonic analysis of the human extrastriate cortex in the region of V5/MT+: a probabilistic, stereotaxic map of area hOc5. Cereb. Cortex. doi:10.1093/cercor/bhj181.

Matelli, M., Luppino, G., Rizzolatti, G., 1991. Architecture of superior and mesial area 6 and the adjacent cingulate cortex in the macaque monkey. J. Comp. Neurol. 311, 445–462.

MCCarthy, G., Spicer, M., Adrignolo, A., Luby, M., Gore, J., Allison, T., 1995. Brain activation associated with visual motion studied by functional magnetic resonance imaging in humans. Hum. Brain Mapp. 2, 234–243.

Mohlberg, H., Weiss, P.H., Fink, G.R., Zilles, K., Amunts, K., 2002. Integration of a new non-linear elastic warping method and SPM99: verbal fluency and cytoarchitecture. NeuroImage 16, 492.

Mohlberg, H., Lerch, J., Amunts, K., Evans, A.C., Zilles, K., 2003. Probabilistic cytoarchitectonic maps transformed into MNI space. Presented at the 9th International Conference on Functional Mapping of the Human Brain, June 19–22 2003, New YorkNeuroImage, vol. 19 (2). Available on CD ROM.

Morosan, P., Rademacher, J., Schleicher, A., Amunts, K., Schormann, T., Zilles, K., 2001. Human primary auditory cortex: cytoarchitectonic subdivisions and mapping into a spatial reference system. NeuroImage 13, 684–701.

Mosher, J.C., Leahy, R.M., 1992. Multiple dipole modeling and localization from spatio-temporal MEG data. IEEE Trans. Biomed. Eng. 39 (6), 541–557.

Mosher, J.C., Leahy, R.M., 1998. Recursive MUSIC: a framework for EEG and MEG source localization. IEEE Trans. Biomed. Eng. 45 (11), 1342–1354.

Pascual-Marqui, R.D., 2002. Standardized low resolution brain electromagnetic tomography (sLORETA): technical details. Methods Find. Exp. Clin. Pharmacol. 24D, 5–12.

Passingham, R.E., Stephan, K.E., Kotter, R., 2002. The anatomical basis of functional localization in the cortex. Nat. Rev., Neurosci. 3 (8), 606–616.

Rademacher, J., Morosan, P., Schormann, T., Schleicher, A., Werner, C., Freund, H.-J., Zilles, K., 2001. Probabilistic mapping and volume measurement of human primary auditory cortex. NeuroImage 13, 669–683.

Roland, P.E., Zilles, K., 1994. Brain atlases—A new research tool. Trends Neurosci. 17, 458–467.

Roland, P.E., Zilles, K., 1998. Structural divisions and functional fields in the human cerebral cortex. Brain Res. Rev. 26, 87–105.

Rottschy, C., Eickhoff, S.B., Schleicher, A., Mohlberg, H., Zilles, K., Amunts, K., 2005. The cytoarchitecture of the ventral extrastriate human visual cortex. Neuroimage Available on CD-Rom: Presented at the 11th International Conference on Functional Mapping of the Human Brain, June 12–16, 2005, Toronto.

Scherg, M., Berg, P., 1996. New concepts of brain source imaging and localization. Electroencephalogr. Clin. Neurophysiol., Suppl. 46, 127–137.

Schleicher, A., Zilles, K., 1990. A quantitative approach to cytoarchitectonics: analysis of structural inhomogeneities in nervous tissue using an image analyzer. J. Microsc. 157, 367–381.

Schleicher, A., Amunts, K., Geyer, S., Morosan, P., Zilles, K., 1999. Observer-independent method for microstructural parcellation of

cerebral cortex: a quantitative approach to cytoarchitectonics. NeuroImage 9, 165–177.

Talairach, J., Tournoux, P., 1988. Coplanar Stereotaxic Atlas of the Human Brain. Thieme, Stuttgart.

Taylor, J.G., Ioannides, A.A., Müller-Gärtner, H.W., 1999. Mathematical analysis of lead field expansions. IEEE Trans. Med. Imag. 18, 151–163.

Tootell, R.B.H., Reppas, J.B., Kwong, K.K., Malach, R., Born, R.T., Brady, T.J., Rosen, B.R., Belliveau, J.W., 1995. Functional analysis of human MT and related visual cortical areas using functional magnetic resonance imaging. J. Neurosci. 15, 3215–3230.

Vigario, R., Sarela, J., Jousmaki, V., Hamalainen, M., Oja, E., 2000. Independent component approach to the analysis of EEG and MEG recordings. IEEE Trans. Biomed. Eng. 47, 589–593.

Wilms, M., Eickhoff, S.B., Specht, K., Amunts, K., Shah, N.J., Malikovic, A., Fink, G.R., 2005. Human V5/MT+: comparison of functional and cytoarchitectonic data. Anat. Embryol. 210, 485–495.

Wohlschlager, A.M., Specht, K., Lie, C., Mohlberg, H., Wohlschlager, A., Bente, K., Pietrzyk, U., Stocker, T., Zilles, K., Amunts, K., Fink, G.R., 2005. Linking retinotopic fMRI mapping and anatomical probability maps of human occipital areas V1 and V2. NeuroImage 15, 73–82.

Young, J.P., Geyer, S., Grefkes, C., Amunts, K., Morosan, P., Zilles, K., Roland, P.E., 2003. Regional cerebral blood flow correlations of somatosensory areas 3a, 3b, 1, and 2 in humans during rest: a PET and cytoarchitectural study. Hum. Brain Mapp. 19, 183–196.

Zeki, S., Watson, J.D.G., Lueck, C.J., Friston, K.J., Kennard, C., Frackowiak, R.S.J., 1991. A direct demonstration of functional specialization in human visual cortex. J. Neurosci. 11, 641–649.

Zilles, K., Schleicher, A., Langemann, C., Amunts, K., Morosan, P., Palomero-Gallagher, N., Schormann, T., Mohlberg, H., Burgel, U., Steinmetz, H., Schlaug, G., Roland, P.E., 1997. Quantitative analysis of sulci in the human cerebral cortex: development, regional heterogeneity, gender difference, asymmetry, intersubject variability and cortical architecture. Hum. Brain Mapp. 5, 218–221.

Zilles, K., Schleicher, A., Palomero-Gallagher, N., Amunts, K., 2002. Quantitative analysis of cyto- and receptor architecture of the human brain. In: Mazziotta, J.C., Toga, A. (Eds.), Brain Mapping: The Methods. Elsevier, USA, pp. 573–602.

4-D Neuroimaging, 1999: MAGNES 2500 WH Software Reference Manual. 4-D Neuroimaging, 9727 Pacific Height Blvd. San Diego, California 92121, USA.